Geophysical Research Letters

RESEARCH LETTER
10.1002/2017GL076821

Key Points:
- A property-conserving, data-constrained ocean state estimate allows study of mechanisms controlling global mean sea surface temperature ($\overline{T}$)
- Advection plays a role in $\overline{T}$ variability at interannual and longer time scales but is not a dominant driver at any scale
- Diffusion does not always act as a simple damping of forcing surface fluxes (e.g., at semiannual time scales)

Correspondence to:
R. M. Ponte,
rponte@aer.com

Citation:
Ponte, R. M., & Piecuch, C. G. (2018). Mechanisms controlling global mean sea surface temperature determined from a state estimate. *Geophysical Research Letters*, *45*, 3221–3227. https://doi.org/10.1002/2017GL076821

Received 15 DEC 2017
Accepted 12 MAR 2018
Accepted article online 25 MAR 2018
Published online 13 APR 2018

Mechanisms Controlling Global Mean Sea Surface Temperature Determined From a State Estimate

R. M. Ponte[1] **and C. G. Piecuch**[1,2]

[1] Atmospheric and Environmental Research, Inc., Lexington, MA, USA, [2] Now at Woods Hole Oceanographic Institution, Woods Hole, MA, USA

Abstract Global mean sea surface temperature ($\overline{T}$) is a variable of primary interest in studies of climate variability and change. The temporal evolution of $\overline{T}$ can be influenced by surface heat fluxes ($\overline{\mathcal{F}}$) and by diffusion ($\overline{\mathcal{D}}$) and advection ($\overline{\mathcal{A}}$) processes internal to the ocean, but quantifying the contribution of these different factors from data alone is prone to substantial uncertainties. Here we derive a closed $\overline{T}$ budget for the period 1993–2015 based on a global ocean state estimate, which is an exact solution of a general circulation model constrained to most extant ocean observations through advanced optimization methods. The estimated average temperature of the top (10-m thick) level in the model, taken to represent $\overline{T}$, shows relatively small variability at most time scales compared to $\overline{\mathcal{F}}$, $\overline{\mathcal{D}}$, or $\overline{\mathcal{A}}$, reflecting the tendency for largely balancing effects from all the latter terms. The seasonal cycle in $\overline{T}$ is mostly determined by small imbalances between $\overline{\mathcal{F}}$ and $\overline{\mathcal{D}}$, with negligible contributions from $\overline{\mathcal{A}}$. While $\overline{\mathcal{D}}$ seems to simply damp $\overline{\mathcal{F}}$ at the annual period, a different dynamical role for $\overline{\mathcal{D}}$ at semiannual period is suggested by it being larger than $\overline{\mathcal{F}}$. At periods longer than annual, $\overline{\mathcal{A}}$ contributes importantly to $\overline{T}$ variability, pointing to the direct influence of the variable ocean circulation on $\overline{T}$ and mean surface climate.

Plain Language Summary Global mean sea surface temperature $\overline{T}$ is a key metric when defining the Earth's climate. Determining what controls the evolution of $\overline{T}$ is thus vital for understanding past climate variability and predicting its future evolution. Processes that control $\overline{T}$ involve forcing surface heat fluxes, as well as advection and diffusion of heat internal to the ocean, but their relative contributions are poorly known and difficult to assess from observations alone. Here we use advanced methods to combine models and data and derive a closed budget for $\overline{T}$ variability in terms of the forcing, advection, and diffusion processes. The estimated $\overline{T}$ shows relatively small variability compared to surface forcing, advection, or diffusion, reflecting the tendency for largely balancing effects from all the latter terms. The seasonal cycle in $\overline{T}$ is mostly determined by small imbalances between forcing and diffusion, with negligible contributions from advection. Diffusion does not always act as a simple damping of forcing surface fluxes, however. In addition, at periods longer than annual, advection contributes importantly to $\overline{T}$ variability. The results point to the direct influence of the variable ocean circulation on $\overline{T}$ and the Earth's surface climate.

1. Introduction

The Earth's mean surface temperature is commonly used to track climate variability and change of importance to society (Intergovernmental Panel on Climate Change, 2014). With approximately two thirds of the planet covered by oceans, estimates of sea surface temperature are a key ingredient in defining mean surface temperature (e.g., Hansen et al., 2010; Karl et al., 2015). Determining what controls the evolution of global mean sea surface temperature is thus vital for understanding past climate change and predicting its future evolution.

Symbolically, conservation of temperature T can be written as

$$T' = \mathcal{A}' + \mathcal{D}' + \mathcal{F}', \tag{1}$$

where primes denote tendency in time, $\mathcal{A}'$, $\mathcal{D}'$ represent temperature tendencies related to advective, diffusive heat fluxes internal to the ocean, and $\mathcal{F}'$ represents temperature tendency due to external forcing heat fluxes, nonzero only near the surface. Understanding mechanisms controlling global mean sea surface temperature ($\overline{T}$) involves quantitative analysis of how surface exchanges of heat with the interior ocean below

and the atmosphere above are mediated by $\mathcal{A}'$, $\mathcal{D}'$, and $\mathcal{F}'$. A number of different regimes are possible. For example, $\overline{T}$ could be primarily driven by surface heat fluxes, with mixing acting to dampen to a lesser or greater extent such influences, or, in contrast, $\overline{T}$ could be controlled by advection processes (e.g., wind-driven Ekman pumping) not necessarily tied to the surface forcing fluxes.

Evaluation of the balances implied in (1) using solely observations is difficult because of uncertainties in data and missing information needed to estimate some budget terms (e.g., Cummins et al., 2016). Models are useful for this purpose (e.g., Gregory, 2000; Wolfe et al., 2008), particularly if they provide a realistic representation of the evolution of $\overline{T}$. An alternative approach, followed in this work, is to use ocean state estimates in which advanced optimization procedures are used to fit an ocean model to most available observations, while retaining conservation principles that allow for a closed heat budget analysis (e.g., Stammer et al., 2016; Wunsch et al., 2009).

Our focus is on assessing the nature of the $\overline{T}$ budget, with particular interest in clarifying whether diffusion acts always as a damping on the forcing, whether advection can noticeably contribute to changes in $\overline{T}$, and more generally how forcing, diffusion, and advection processes relate to each other as a function of time scale and combine to produce observed changes in $\overline{T}$. These efforts complement recent modeling and observational studies that have examined vertical ocean heat transports primarily below the surface and focusing for the most part on steady or longest time scale balances (Cummins et al., 2016; Griffies et al., 2015; Liang et al., 2015, 2017).

2. Tools and Methods

For budget diagnostics of $\overline{T}$, we use a recent global ocean state estimate (Forget et al., 2015; Fukumori et al., 2017) produced by the project for Estimating the Circulation and Climate of the Ocean (ECCO; Wunsch et al., 2009). The solution, named ECCO Version 4 Release 3 (hereafter Ev4r3), is described in detail by Fukumori et al. (2017) and Forget et al. (2015), with fields and documentation available at ftp://ecco.jpl.nasa.gov/Version4/Release3/. The estimate covers the period 1992–2015 and is provided on a global horizontal grid, with nominal spacing ~0.25°–1°, on 50 vertical levels with 10-m spacing near the surface. As a brief summary of general characteristics, Ev4r3 is a solution of the Massachusetts Institute of Technology general circulation model (MITgcm) constrained to satellite data (altimeter, gravity, sea surface temperature, and salinity) and in situ hydrography (Argo, XBTs, CTDs, and marine mammals). The optimization and data fitting, done iteratively using the method of Lagrange multipliers, are achieved by changes in initial and surface boundary conditions, as well as in mixing coefficients. The final estimate is thus based on a free forward run of the MITgcm with adjusted parameters and, key for our purposes, yields conserved tracer fields within numerical precision (Piecuch, 2017).

We examine in detail the global mean temperature budget for the top level in Ev4r3, taken to represent $\overline{T}$. Surface budget analyses are often formulated in terms of mixed layer temperature (e.g., Buckley et al., 2014). By focusing on the top level instead, we explicitly assess processes internal to the mixed layer, as represented in coarse-resolution models as used in Ev4r3, and whether a balance between mixing and forcing is always predominant. Budget analyses over thicker surface control volumes (upper 100 and 200 m) are also considered to contrast with and elucidate the nature of the $\overline{T}$ budget.

Monthly mean fields for the period 1993–2015 form the basis of the analysis (first year is not used to avoid initial transients and partial altimeter data coverage, which only starts in October 1992). Budget calculations follow the detailed steps in Piecuch (2017). For the MITgcm configuration used in Ev4r3, the conservation of potential temperature θ is given by (see equation (4) of Forget et al., 2015)

$$\underbrace{\frac{\partial\left(s^{*}\theta\right)}{\partial t}}_{\overline{T}'}=\underbrace{-\nabla_{z^{*}}\left(s^{*}\theta\mathbf{v}_{\mathrm{res}}\right)-\frac{\partial\left(\theta w_{\mathrm{res}}\right)}{\partial z^{*}}}_{\mathcal{A}'}+\underbrace{s^{*}D_{\theta}}_{\mathcal{D}'}+\underbrace{s^{*}\mathcal{F}_{\theta}}_{\mathcal{F}'}. \tag{2}$$

Here $\mathbf{v}_{\mathrm{res}}=(u_{\mathrm{res}},v_{\mathrm{res}})$ and w_{res} are the horizontal and vertical residual mean velocities, respectively, composed of both the resolved (Eulerian) flow field, as well as the "bolus" velocity, parameterizing unresolved eddy effects after Gent and McWilliams (1990). The term D_{θ} represents parameterized diffusive mixing processes, including the mixed layer scheme of Gaspar et al. (1990), isopycnal diffusion of Redi (1982), as well as the effects of background interior diffusion and convective adjustment. Forcing $\mathcal{F}_{\theta}$ represents the net effects

Table 1
Trends and Annual and Semiannual Cycles

	Trend	Annual		Semiannual	
	(°C/year)	A	ϕ	A	ϕ
$\overline{T}$ (data)	9.4×10^{-3}	0.11	328	0.12	339
$\overline{T}$ (Ev4r3)	4.9×10^{-3}	0.14	4	0.13	342
$\overline{\mathcal{F}}$	−28.78	1.27	15	0.34	191
$\overline{\mathcal{D}}$	23.51	1.12	194	0.47	2
$\overline{\mathcal{A}}$	5.27	0.04	257	0.01	145
$\overline{T}_{200}$	4.0×10^{-3}	0.08	9	0.02	196
$\overline{\mathcal{F}}_{200}$	1.7×10^{-3}	0.08	11	0.02	195
$\overline{\mathcal{D}}_{200}$	4.57×10^{-2}	<0.005	126	<0.005	280
$\overline{\mathcal{A}}_{200}$	-4.34×10^{-2}	0.01	297	<0.005	143

Note. Values are based on a joint least squares fit of the time series for trend plus annual and semiannual cycles. The latter correspond to a fit of the form $A \sin[\omega(t - t_0) + \phi\pi/180]$, where A is amplitude in °C, ϕ is phase in degrees, ω is frequency, and t_0 is starting date of 1 January 1993. Estimates based on 0–200-m budgets are denoted by subscript 200.

of latent, sensible, longwave, and shortwave surface heat flux components, plus a (small) contribution from heat content carried by precipitation. These terms only affect the top level, except the shortwave component, which decays exponentially from the surface down to 200 m (Piecuch, 2017). Lastly, the scaling factor $s^* = 1 + \eta/H$, where η is sea level and H is depth, and enters the definition of the stretched vertical coordinate $z^* = (z - \eta)/s^*$ used by the MITgcm.

No attempt is made here to separate all the different components within each budget term in (2). The four fields in (2) are spatially averaged and integrated in time to produce global (area weighted) mean quantities ($\overline{T}$, $\overline{\mathcal{A}}$, $\overline{\mathcal{D}}$, and $\overline{\mathcal{F}}$), and budget results are thus presented in temperature space for direct interpretation of $\overline{T}$ variability as a function of time scale. For comparison with the Ev4r3 field, we also use estimates of $\overline{T}$ obtained by globally averaging the satellite-based product of Reynolds et al. (2002). Comparisons are not intended as an independent check on the Ev4r3 estimate, since the solution is also constrained by the Reynolds et al. (2002) product, but simply provide a measure of fit.

3. Budget Analyses

3.1. Trends, Seasonal, and Nonseasonal Variability

Linear trends are commonly studied in climate analysis and here can provide insight on the longest time scales present in the record. Values in Table 1 indicate positive trends in $\overline{T}$. The Ev4r3 estimate is about half of that based on the Reynolds et al. (2002) data. Both are extremely small compared to the trends implied by $\overline{\mathcal{F}}$, $\overline{\mathcal{D}}$, or $\overline{\mathcal{A}}$, indicating that contemporary $\overline{T}$ trends represent a small deviation from steady state, time mean balance. Effects of $\overline{\mathcal{F}}$ to strongly decrease $\overline{T}$ are mostly balanced by $\overline{\mathcal{D}}$ (~80% of the magnitude of $\overline{\mathcal{F}}$), but contributions from $\overline{\mathcal{A}}$ at 20% of $\overline{\mathcal{F}}$ are not negligible. The positive $\overline{T}$ trend thus results from a slightly larger warming tendency provided by $\overline{\mathcal{D}}$ and $\overline{\mathcal{A}}$.

One expects a warming ocean to be gaining instead of losing heat from surface fluxes, but recall that $\overline{\mathcal{F}}$ only includes the shortwave radiative flux effects on the top level. Although such flux decays with depth down to 200 m, it adds a considerable amount of net heat to the subsurface levels. Budget results for 0–200-m control volume (Table 1) indeed show a small warming trend contribution by $\overline{\mathcal{F}}$. Trends from $\overline{\mathcal{D}}$ and $\overline{\mathcal{A}}$ are also much reduced but an order of magnitude larger than $\overline{\mathcal{F}}$. Trend results in Table 1 thus indicate that both mixing and advection play a key role in fluxing heat vertically near the surface and in maintaining the relative small warming trend.

The detrended $\overline{T}$ time series estimated by Ev4r3 compares well in magnitude and phase with similarly detrended observed series calculated from Reynolds et al. (2002; Figure 1); correlation coefficient between the two series is 0.90. In terms of variability, $\overline{T}$ series in Figure 1 shows a clear seasonal cycle with peak-to-peak monthly variations of ~0.5°C and both an annual and semiannual component, superposed on longer time

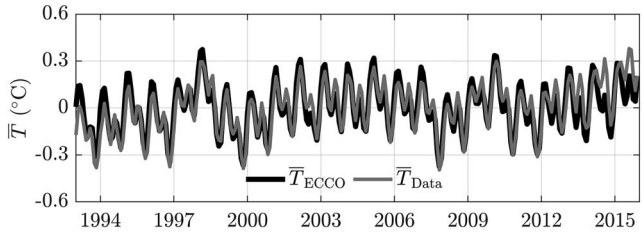

Figure 1. Time series of global mean sea surface temperature $\overline{T}$ estimated from Ev4r3 and from data product of Reynolds et al. (2002).

scale fluctuations. Maximum $\overline{T}$ coincides with the 1997–1998 El Niño and minimum with the 2007–2008 La Niña.

Analysis of $\overline{\mathcal{F}}$, $\overline{\mathcal{D}}$, and $\overline{\mathcal{A}}$ terms can begin to elucidate the causes of such variability in $\overline{T}$. To scrutinize the nature of the dominant seasonal budget in detail, we create a mean seasonal cycle by averaging all January, …, December values. Although compensating annual components seem to dominate $\overline{\mathcal{F}}$ and $\overline{\mathcal{D}}$, the residual also shows a semiannual component (Figure 2a). The mean seasonal cycle in $\overline{T}$ clearly results from the balance between $\overline{\mathcal{F}}$ and $\overline{\mathcal{D}}$, with $\overline{\mathcal{A}}$ being negligible (Figure 2). Such balance holds for both the annual and semiannual components (Table 1).

Annual and semiannual amplitudes in $\overline{T}$ are very similar (Table 1) but the nature of the $\overline{\mathcal{F}}$, $\overline{\mathcal{D}}$ balance is noticeably different. In particular, while annual amplitude of $\overline{\mathcal{F}}$ is larger than $\overline{\mathcal{D}}$, the reverse is true for the semiannual cycle. The larger semiannual amplitude of $\overline{\mathcal{D}}$ compared to $\overline{\mathcal{F}}$ indicates that mixing does not always act simply as a damping of the forcing fluxes near the surface and can be more dynamically involved in causing variability in $\overline{T}$.

The approximately equal amplitudes of annual and semiannual cycles hold mostly near the surface. Considering budgets for thicker layers leads to a relatively smaller semiannual cycle; annual to semiannual amplitude ratio is ~4 for 0–200-m budgets (Table 1), and 0–100-m results are similar (not shown). The prominent semiannual cycle in $\overline{T}$ is thus primarily a very shallow signal. In addition, as expected when integrating over more of the mixed layer, for 0–200-m budgets the effects of $\overline{\mathcal{D}}$ become much less important and the temperature variability basically follows $\overline{\mathcal{F}}$ (Table 1). In any case, influence of $\overline{\mathcal{A}}$ is still relatively weak, regardless of whether one considers the top level or deeper control volumes.

Removing annual and semiannual terms to focus on nonseasonal behavior, typical variations in $\overline{T}$ range from ~0.1°C at monthly time scales to ~0.4°C at interannual time scales (Figure 3a), with the latter clearly linked to El Niño and La Niña events (e.g., highs in 1997–1998, 2009–2010, 2015, and lows in 2000 and 2008). The budget terms (Figure 3a) still reveal a strong tendency for anticorrelation and compensation between $\overline{\mathcal{F}}$ and $\overline{\mathcal{D}}$, as with the seasonal cycle, but now with $\overline{\mathcal{A}}$ being as important at the longest (decadal) time scales. There is also compensation evident between $\overline{\mathcal{A}}$ and $\overline{\mathcal{D}}$ at the longest scales. Nonseasonal $\overline{T}$ variability is thus somewhat weaker than that implied by any of the balancing budget terms. Consideration of thicker control volumes (e.g., 0–200 m; Figure 3b) leads to a weakening of the role played by $\overline{\mathcal{D}}$ and a somewhat different evolution of the various budget terms, but $\overline{\mathcal{A}}$ remains important at interannual and longer time scales.

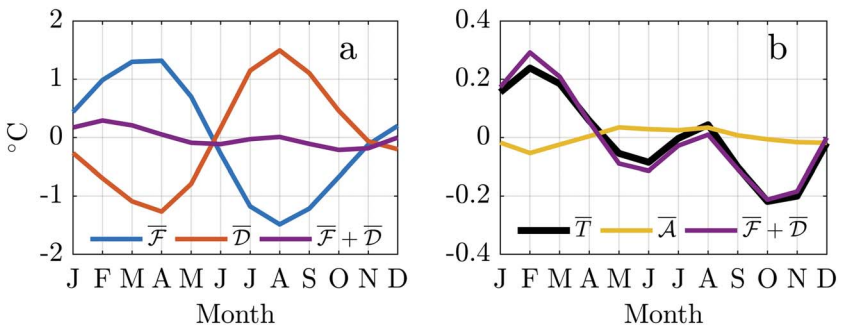

Figure 2. (a) Mean seasonal cycle in $\overline{\mathcal{F}}$ and $\overline{\mathcal{D}}$, and their sum $\overline{\mathcal{F}}+\overline{\mathcal{D}}$. (b) Mean seasonal cycle in $\overline{T}$, $\overline{\mathcal{A}}$, and $\overline{\mathcal{F}}+\overline{\mathcal{D}}$.

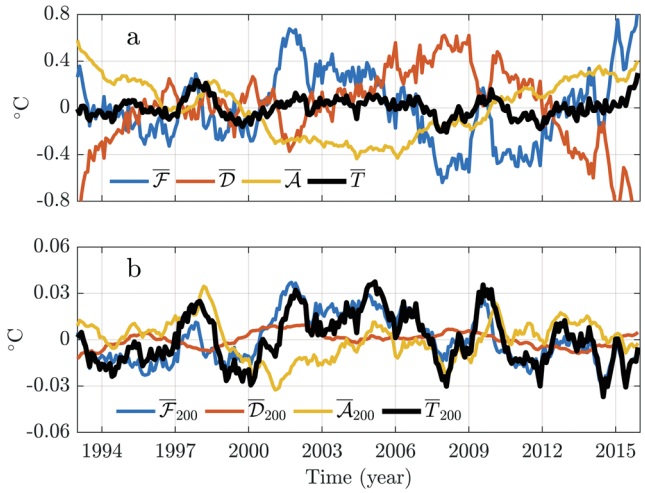

Figure 3. (a) Values of $\overline{\mathcal{F}}$, $\overline{\mathcal{D}}$, and $\overline{\mathcal{A}}$, as well as global mean temperature $\overline{T}$, with the trend and annual and semiannual cycles removed. (b) As in (a) but for values corresponding to the 0–200-m budget.

3.2. Spectral Analysis

Coherence and admittance analyses provide a quantitative way of summarizing the nature of the $\overline{T}$ budget as a function of time scale (Figure 4). A main balance between $\overline{\mathcal{F}} + \overline{\mathcal{D}}$ and $\overline{T}$ should result in high coherence between the series and an admittance amplitude ~1 with near-zero phase difference. This is indeed the case at annual and semiannual periods, for which surface forcing is strongest, but deviations from that behavior are seen at other periods (Figures 4a–4c). Such deviations reflect the nonnegligible effect of $\overline{\mathcal{A}}$, most apparent at periods longer than annual, which is consistent with what is inferred from the trend analysis in Table 1.

Power spectra can further quantify relative magnitudes of $\overline{T}$, $\overline{\mathcal{F}}$, $\overline{\mathcal{D}}$, and $\overline{\mathcal{A}}$ (Figure 5). At all periods, power in $\overline{T}$ tends to be small compared to (for the most part balancing) effects of $\overline{\mathcal{F}}$, $\overline{\mathcal{D}}$, and $\overline{\mathcal{A}}$. In particular, power

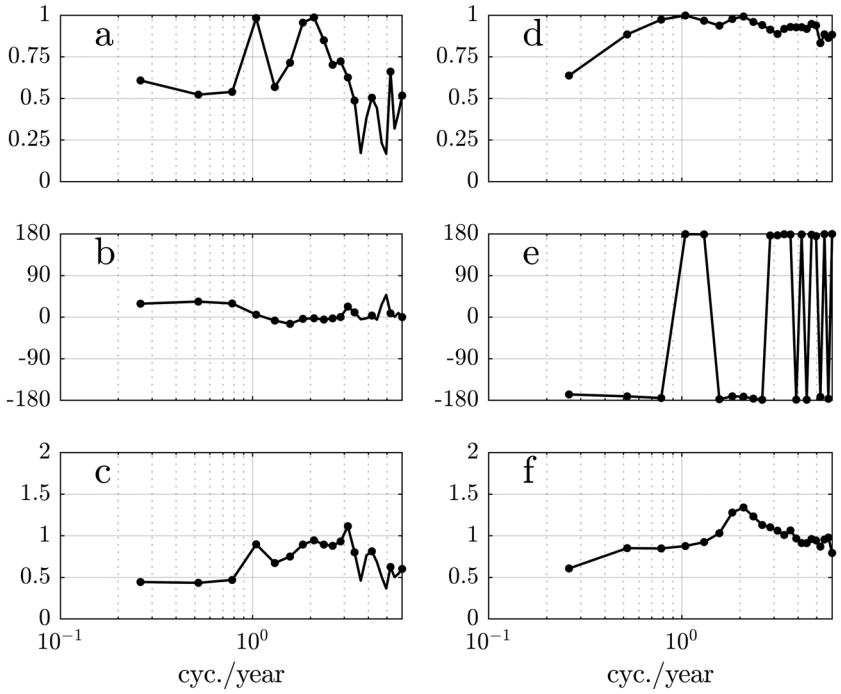

Figure 4. Coherence amplitude, coherence phase, and admittance amplitude for the pairs ($\overline{T}$, $\overline{\mathcal{F}} + \overline{\mathcal{D}}$; a–c) and ($\overline{\mathcal{D}}$,$\overline{\mathcal{F}}$; d–f). Admittance is calculated as P_{xy}/P_{xx} where P is cross-power spectral density, and x is $\overline{\mathcal{F}} + \overline{\mathcal{D}}$ (c) and $\overline{\mathcal{F}}$ (f). Circles denote frequencies for which coherence is significantly different from zero at the 95% confidence level.

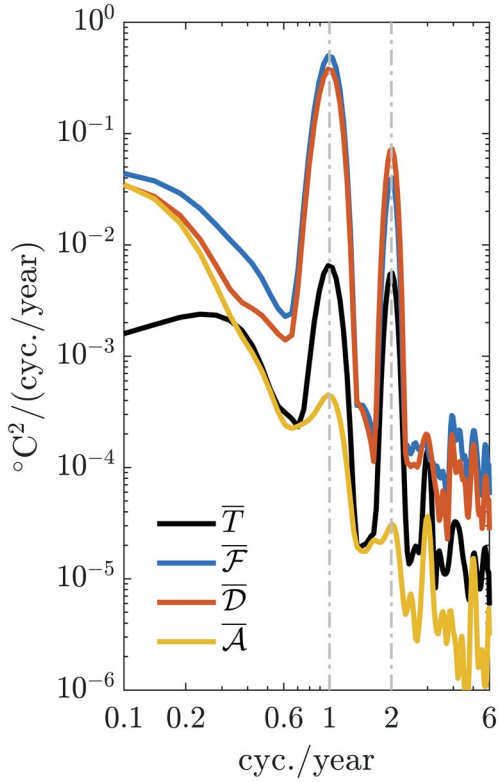

Figure 5. Power spectral density for $\overline{T}$, $\overline{\mathcal{F}}$, $\overline{\mathcal{D}}$, and $\overline{\mathcal{A}}$ from Ev4r3. Vertical dash-dotted lines mark the annual and semiannual periods.

in $\overline{\mathcal{A}}$ is comparable or larger than that in $\overline{T}$ at periods longer than 1 year. There is, however, no evidence for a dominant role of $\overline{\mathcal{A}}$ in setting variability in $\overline{T}$ (i.e., no periods show $\overline{\mathcal{A}}$ of the same magnitude as $\overline{T}$ and much larger than $\overline{\mathcal{F}}$ and $\overline{\mathcal{D}}$).

Analyzing the relation between $\overline{\mathcal{F}}$ and $\overline{\mathcal{D}}$ in more detail (Figures 4d–4f), we find that the two terms are nearly out of phase over all periods. The coherence between $\overline{\mathcal{F}}$ and $\overline{\mathcal{D}}$ is strong at most periods but drops off at the longest time scales resolved, where the relation between all terms in the $\overline{T}$ budget becomes more involved and includes $\overline{\mathcal{A}}$ as well. In addition, admittance amplitudes are ~1 except again at the longest periods and also near the semiannual band. At the latter time scale, admittance amplitude greater than one is consistent with more power in $\overline{\mathcal{D}}$ than in $\overline{\mathcal{F}}$ (see respective spectra in Figure 5, also Table 1), which does not support the view of $\overline{\mathcal{D}}$ having a simple damping role on $\overline{\mathcal{F}}$, as already noted.

4. Concluding Remarks

Analysis of the $\overline{T}$ budget in the property-conserving, energetically consistent Ev4r3 ocean state estimate reveals large annual and semiannual $\overline{T}$ signals superposed on longer time scale variations. The annual cycle is primarily driven by surface heat fluxes and damped by diffusion. The semiannual cycle is more complex, with diffusion playing more than a damping role in the budget. At time scales longer than annual, advection plays an important (but not dominant) role in $\overline{T}$ variability, a result which is robust to consideration of budgets for thicker near-surface control volumes.

Apart from good estimates of the surface heat fluxes, the need to account for both mixing and advection processes in the upper ocean seems warranted for realistically simulating the evolution of $\overline{T}$ at interannual and longer time scales. Knowledge of surface winds and the wind-driven near-surface circulation is likely important for accurate representation of advection processes. The results indicate the role of ocean dynamics in exerting control over variability in $\overline{T}$ and mean surface climate on time scales as short as interannual.

Our findings hold for the Ev4r3 estimate, with its particular subgrid scale parameterizations of mixing physics. Although the estimate tracks observed $\overline{T}$ variability within expected uncertainties, a legitimate question

is how the balances found in Ev4r3 might depend on assumed mixed layer physics and on other model details more generally. Recent comparisons of surface heat flux products (Liang & Yu, 2016) indicate the realism of our $\overline{\mathcal{F}}$ estimates, but we are not aware of any published estimates of $\overline{\mathcal{A}}$, $\overline{\mathcal{D}}$ for comparison with our results. In this regard, similar budget calculations with different ocean models or, better yet, with coupled climate models that produce reasonable $\overline{T}$ behaviors would be very helpful for comparison. The importance of having appropriate model diagnostics to conduct relevant heat budget analyses needs to be emphasized (Griffies et al., 2016).

Many other questions remain to be explored. For example, it is important to decompose $\overline{\mathcal{F}}$ into turbulent and radiative components and examine each term individually, for more insight on what sets the behavior of $\overline{\mathcal{F}}$ in relation to $\overline{T}$. Similarly, several aspects of $\overline{\mathcal{A}}$ need to be clarified, including a better understanding of how $\overline{\mathcal{A}}$ may be related to wind-driven currents and quantifying the separate contributions to $\overline{\mathcal{A}}$ from resolved flows and parameterized bolus transports. Ultimately, regional analyses will be needed to understand the behavior of the global mean budget (e.g., the different relation between $\overline{\mathcal{F}}$ and $\overline{\mathcal{D}}$ in the annual and semiannual cycles). Relating large regional variability to the (small residual) global means requires rigorous treatment of all budget terms as attempted here. While examination of these and other issues is deferred to future work, we hope the current analysis can stimulate further interest in the need to understand what controls variability in $\overline{T}$ and how relevant mechanisms can be well represented in ocean and climate models.

Acknowledgments
Work was carried out under the ECCO project, funded by the NASA Physical Oceanography, Cryospheric Science, and Modeling, Analysis and Prediction programs. Additional support was provided by NSF grant PLR-1513396. Original data and Ev4r3 output used in this work are available as described in the text and references.

References

Buckley, M. W., Ponte, R. M., Forget, G., & Heimbach, P. (2014). Low-frequency SST and upper-ocean heat content variability in the North Atlantic. *Journal of Climate*, *27*(13), 4996–5018. https://doi.org/10.1175/JCLI-D-13-00316.1

Cummins, P. F., Masson, D., & Saenko, O. A. (2016). Vertical heat flux in the ocean: Estimates from observations and from a coupled general circulation model. *Journal of Geophysical Research: Oceans*, *121*, 3790–3802. https://doi.org/10.1002/2016JC011647

Forget, G., Campin, J.-M., Heimbach, P., Hill, C. N., Ponte, R. M., & Wunsch, C. (2015). ECCO version 4: An integrated framework for non-linear inverse modeling and global ocean state estimation. *Geoscientific Model Development*, *8*, 3071–3104. https://doi.org/10.5194/gmd-8-3071-2015

Fukumori, I., Wang, O., Fenty, I., Forget, G., Heimbach, P., & Ponte, R. M. (2017). ECCO version 4 release 3. Pasadena, CA: Jet Propulsion Laboratory. Retrieved from http://hdl.handle.net/1721.1/110380, https://doi.org/1721.1/110380, ftp://ecco.jpl.nasa.gov/Version4/Release3/doc/v4r3_estimation_synopsis.pdf

Gaspar, P., Grégoris, Y., & Lefevre, J.-M. (1990). A simple eddy kinetic energy model for simulations of the oceanic vertical mixing: Tests at station Papa and long-term upper ocean study site. *Journal of Geophysical Research*, *95*(C9), 16,179–16,193. https://doi.org/10.1029/JC095iC09p16179

Gent, P. R., & McWilliams, J. C. (1990). Isopycnal mixing in ocean circulation models. *Journal of Physical Oceanography*, *20*(1), 150–155. https://doi.org/10.1175/1520-0485(1990)020<0150:IMIOCM>2.0.CO;2

Gregory, J. M. (2000). Vertical heat transports in the ocean and their effect on time-dependent climate change. *Climate Dynamics*, *16*(7), 501–515. https://doi.org/10.1007/s003820000059

Griffies, S. M., Winton, M., Anderson, W. G., Benson, R., Delworth, T. L., Dufour, C. O., et al. (2015). Impacts on ocean heat from transient mesoscale eddies in a hierarchy of climate models. *Journal of Climate*, *28*(3), 952–977. https://doi.org/10.1175/JCLI-D-14-00353.1

Griffies, S. M., Danabasoglu, G., Durack, P. J., Adcroft, A. J., Balaji, V., Böning, C. W., et al. (2016). OMIP contribution to CMIP6: Experimental and diagnostic protocol for the physical component of the Ocean Model Intercomparison Project. *Geoscientific Model Development*, *9*(9), 3231–3296. https://doi.org/10.5194/gmd-9-3231-2016

Hansen, J., Ruedy, R., Sato, M., & Lo, K. (2010). Global surface temperature change. *Reviews of Geophysics*, *48*, rG4004. https://doi.org/10.1029/2010RG000345

Intergovernmental Panel on Climate Change (2014). Climate Change 2014: Synthesis Report. Contribution of Working Groups I, II and III to the Fifth Assessment Report of the Intergovernmental Panel on Climate Change (151 pp.). Geneva, Switzerland: Geneva, Switzerland: IPCC.

Karl, T. R., Arguez, A., Huang, B., Lawrimore, J. H., McMahon, J. R., Menne, M. J., et al. (2015). Possible artifacts of data biases in the recent global surface warming hiatus. *Science*, *348*(6242), 1469–1472. https://doi.org/10.1126/science.aaa5632

Liang, X., & Yu, L. (2016). Variations of the global net air-sea heat flux during the "hiatusperiod" (2001–10). *Journal of Climate*, *29*(10), 3647–3660. https://doi.org/10.1175/JCLI-D-15-0626.1

Liang, X., Wunsch, C., Heimbach, P., & Forget, G. (2015). Vertical redistribution of oceanic heat content. *Journal of Climate*, *28*(9), 3821–3833. https://doi.org/10.1175/JCLI-D-14-00550.1

Liang, X., Piecuch, C. G., Ponte, R. M., Forget, G., Wunsch, C., & Heimbach, P. (2017). Change of the global ocean vertical heat transport over 1993–2010. *Journal of Climate*, *30*(14), 5319–5327. https://doi.org/10.1175/JCLI-D-16-0569.1

Piecuch, C. G. (2017). A note on practical evaluation of budgets in ECCO version 4 release 3 (Tech Rep.). Lexington, MA: Atmospheric and Environmental Research, Inc. Retrieved from ftp://ecco.jpl.nasa.gov/Version4/Release3/doc/v4r3_budgets_howto.pdf

Redi, M. H. (1982). Oceanic isopycnal mixing by coordinate rotation. *Journal of Physical Oceanography*, *12*(10), 1154–1158. https://doi.org/10.1175/1520-0485(1982)012<1154:OIMBCR>2.0.CO;2

Reynolds, R. W., Rayner, N. A., Smith, T. M., Stokes, D. C., & Wang, W. (2002). An improved in situ and satellite SST analysis for climate. *Journal of Climate*, *15*(13), 1609–1625. https://doi.org/10.1175/1520-0442(2002)015<1609:AIISAS>2.0.CO;2

Stammer, D., Balmaseda, M., Heimbach, P., Köhl, A., & Weaver, A. (2016). Ocean data assimilation in support of climate applications: Status and perspectives. *Annual Review of Marine Science*, *8*(1), 491–518. https://doi.org/10.1146/annurev-marine-122414-034113

Wolfe, C. L., Cessi, P., McClean, J. L., & Maltrud, M. E. (2008). Vertical heat transport in eddying ocean models. *Geophysical Research Letters*, *35*, L23605. https://doi.org/10.1029/2008GL036138

Wunsch, C., Heimbach, P., Ponte, R. M., & Fukumori, I. (2009). The global general circulation of the ocean estimated by the ECCO consortium. *Oceanography*, *22*(2), 88–103. https://doi.org/0.5670/oceanog.2009.41